DOI: 10.1784/cm2023.1d3

Condition Monitoring of Pitting Evolution Using Multiple Sensing

Zaihao Tian
University of Southampton, SO17 1BJ, Southampton, UK
E-mail: z.tian@soton.ac.uk

Shuncai Wang
University of Southampton, SO17 1BJ, Southampton, UK

Daniel Merk
Schaeffler Technologies AG & Co. KG, Georg-Schäfer-Str. 30, 97421, Schweinfurt, Germany

Robert J K Wood
University of Southampton, SO17 1BJ, Southampton, UK

Abstract

Pitting on surfaces is a type of rolling contact fatigue (RCF) occurs in rolling-sliding contacts operating under mixed or boundary lubrication conditions. The early detection of pitting is of great importance due to its potential detrimental effects on the performance and reliability of machinery components, such as rolling element bearings and gears. This research aims to investigate the responses of multiple sensors to the progression of pitting and achieve early detection of pitting initiation.

Experiments were conducted on a TE74 twin-disc tribometer to investigate the behaviour of bearing steel discs. Mild wear and pitting fatigue were obtained with specimens of different roughness combinations. During testing, vibration, acoustic emission (AE) and electrostatic (ES) data were recorded, and post-test signal analysis was conducted in both the time domain and frequency domain. After testing, the worn surfaces were examined to determine the mechanisms responsible for specific features seen in the sensor data.

The presence of pitting in the near-surface region was observed, and its development was effectively monitored using the employed sensing techniques. The stages of running-in, pitting initiation, and pitting formation were identified through the analysis of time-domain parameters and frequency spectrums. Vibration signal analysis exhibited a more prominent indication of pitting formation, whereas AE and ES methods demonstrated an ability to detect the onset of pitting at an earlier stage.

1. Introduction

Rolling element bearings find widespread application in various rotating machinery, where their selection and the precision of associated components significantly impact the successful and reliable operation of the machinery. Despite proper installation and maintenance, rolling contact fatigue (RCF) remains a common failure mode for these bearings. RCF refers to damage caused by repetitive rolling or rolling-sliding contact between metallic surfaces. Fatigue cracks can initiate at localised areas of stress concentration on the surface or within the subsurface, and they propagate due to the cyclic loading. This phenomenon eventually leads to the loss of material, known as pitting or macropitting. Pitting roughens the desired smooth surface of the bearing and if allowed

to run, the rolling surfaces continue to experience increased wear and disruption, ultimately resulting in catastrophic failure [1].

Hence, it is crucial to identify the emergence of incipient RCF at the early stage to prevent catastrophic machinery failures and allow appropriate interventions. Monitoring the vibration signal is widely acknowledged as an effective approach for detecting structural defects in rotating machine components due to its ability to capture dynamic information. This sensing technology has been extensively employed in RCF and wear tests for detecting and diagnosing localised faults in rolling element bearings and gears [2, 3]. In recent decades, acoustic emission (AE) has emerged as another notable sensing technology for structural health monitoring, specifically in the detection of early-stage damage. AE relies on the propagation of elastic stress waves, which may be released due to crack propagation, micropitting, and pitting [4-6]. In contrast to vibration analysis, AE measurements exhibit higher sensitivity to incipient damages, whereas normally substantial damage is required to noticeably affect the vibration properties [4, 7].

During the past three decades, electrostatic (ES) sensing technology has been well developed and applied in various fields, including on-line particle sizing, radial vibration measurement of mechanical systems, and mechanical wear [8]. When being employed as a condition monitoring method, this technique offers several advantages, including high sensitivity and direct measurement of surface changes. These features are particularly valuable for the early detection of machine degradation [8]. ES has been used in various tribological experiments to monitor the onset and propagation of machinery component deterioration [9-11]. These research findings have demonstrated a strong correlation between the electrostatic charge level and the occurrence of fatigue and wear.

Sensor data can be influenced by the machine's structure and compounded by interference from other equipment and structural resonances. Consequently, the interpretation of sensor data is often challenging. The effectiveness of fault detection and diagnosis relies heavily on the techniques employed to extract fault-related information from the acquired signals [2]. The Empirical Model Decomposition (EMD) approach proposed by Huang et al. [12] is a widely used method for analysing non-stationary signals in the time-frequency domain. As a result, the EMD approach has gained significant attention in the field of equipment fault diagnosis. Envelope analysis is a widely recognised signal processing technique utilized for the detection of incipient faults. The notable advantage of envelope analysis lies in its capability to extract periodic impacts from the modulated random noise generated by the damaged sites. Consequently, this technique is frequently employed to identify early damage in machinery components [2, 13, 14].

In the current literature, many studies have been focused on the detection of artificial defects or late stages of fault formation. However, the use of online sensing for effectively monitoring the initiation of RCF has been limited due to the relatively weak signals generated during this stage. The innovative contribution of this works is the construction of a multi-sensing system that enabled the comprehensive detection of pitting evolution. By incorporating data from multiple sensors, a more holistic understanding of the pitting process was obtained and the early detection of pitting initiation was achieved.

The paper is structured into several sections. Section 2 provides details on the specimens, the instrumentation, and the data processing methods. Section 3 presents the experimental results and discussion, which are divided mainly into analysis of the evolution and

mechanism of pitting, and interpretation of data collected from multiple sensors. In Section 4, the paper concludes the sensors' effectiveness in monitoring pitting evolution.

2. Test Methodology

2.1. Experimental Equipment and Materials

In this work, experiments were conducted on a Phoenix Tribology TE74 twin-disc tribometer as shown in Figure. 1 (a). TE74 is a research tribometer that allows wear and RCF to be studied under rolling/sliding conditions. The test rig incorporates two-disc specimens mounted on parallel shafts which can be driven independently, allowing sliding to be induced to the contact by controlling the rotational speed of the specimens. Load can be applied to the contact through the action of a pivot mounted on the load arm.

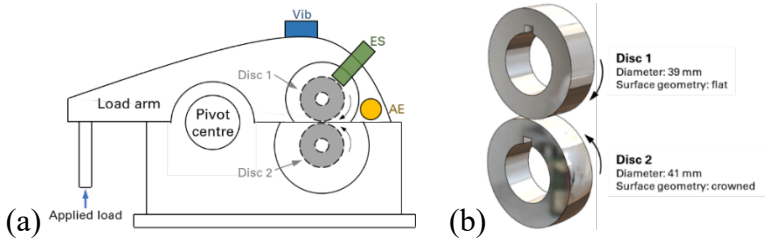

Figure 1. (a) An illustration of TE74 tribometer and specimen locations (b) Schematic drawing of twin-disc specimens

The specimens mounted in TE74 were discs made of AISI 52100 bearing steel. They were 39 mm diameter, 12 mm width cylindrical discs and 41 mm diameter, 12 mm width crowned discs with a transverse diameter of 100 mm as illustrated in Figure. 1 (b). This configuration resulted in a self-aligning elliptical contact geometry which avoided edge stresses while also allowed wear tracks to be in central positions so that the fatigue damage can be detected and observed easily. The 39 mm diameter discs were mounted on the upper specimen shaft and the 41 mm diameter discs on the lower specimen shaft. For the sake of clarity, "Disc 1" is used to denote the 39 mm diameter discs, while "Disc 2" is used to denote the 41 mm diameter discs in the subsequent discussions. The lubricant used was PAO8 oil, a type of synthetic lubricating oil commonly used in applications such as high-performance engines and gearboxes.

2.2. Sensing Instrumentation

As illustrated in Figure 1 (a), three sensors, vibration (Vib), acoustic emission (AE), and electrostatic (ES) sensors were used in this work. An A/20 vibration accelerometer, manufactured by DJ Birchell Company, was fixed at the top of the load arm using adhesive bonding as shown in Figure 2 (a). Vibration data were collected continuously with a sampling rate of 3 kHz. The sensor was connected to a Kistler LabAmp 5165A charge amplifier with an amplification ratio of 0.05 V/pC. Furthermore, the charge amplifier was interfaced with a NI DAQ USB 6002 data acquisition card.

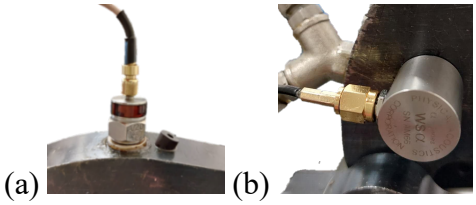

Figure 2. (a) Vibration accelerometer (b) Acoustic emission sensor

The acoustic emission (AE) sensor was a PAC WSα single-ended wideband sensor provided by MISTRAS Group, Inc. The sensor was fixed using epoxy to the load arm. It was connected to a PAC 2/4/6 series pre-amplifier with a gain of 60 dB, and the pre-amplifier was connected to a PCI-2 data acquisition/processing card. AE data was recorded in burst samples of 1 second length with a sampling rate of 2 MHz.

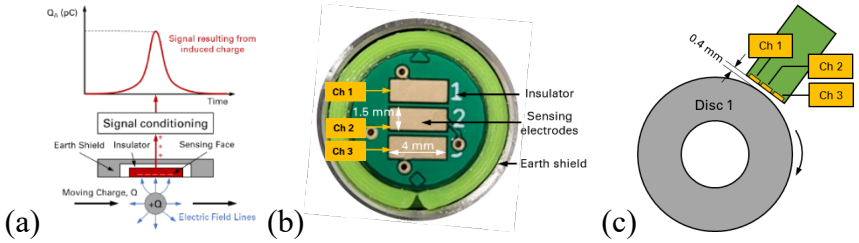

Figure 3. (a) Schematic of electrostatic sensing system (b) ES sensor face (c) Relative positions of the ES sensor and Disc 1

The principle of electrostatic sensing system is illustrated in Figure 3 (a). When a charged particle passes in front of the sensor face, some of the electric lines resulting from the charge terminate on the sensor face. This causes the electrons in the sensor face to redistribute, creating a current flow to balance the additional charge in the vicinity of the sensor [11]. The signal conditioner detects and converts the induced charge into a measurable voltage signal. A 3-channel electrostatic array sensor was used in this work. The sensor comprises three electrodes with a width of 4 mm and a height of 1.5 mm on its face, marked as Ch 1, Ch 2, and Ch 3, as illustrated in Figure 3 (b). The ES sensor was incorporated into the test rig by holes drilled through the load arm to detect surface charge on Disc 1. The relative positions of the electrostatic sensor and Disc 1 are shown in Figure 3 (c). The distance between the centre of the sensor face and Disc 1 was set to 0.4 mm. Considering that Ch 2 was positioned at the centre of the sensor face and the surface geometry of the disc was curved, it maintains the closest proximity to the disc surface, enabling more effective collection of the induced surface charge. Consequently, the analysis was exclusively conducted on signals obtained from Ch 2. The ES data was collected continuously with a sampling rate of 3 kHz. The sensor was connected to the Kistler charge amplifier with an amplification ratio of 1 V/pC and the charge amplifier was interfaced with the NI data acquisition card.

2.3. Data Processing Methods

The raw signals from the three sensors were denoised using the empirical model decomposition (EMD) method. EMD is specifically designed to analyse nonstationary signals by decomposing them into intrinsic mode functions (IMFs) and residual [12]. The IMFs capture the distinct frequency components, while the residual represents the average trend of the signal. To select the denoised signal, energy values of all IMFs were calculated, and the IMFs with the highest values were chosen as the desired signals.

The denoised sensor data was analysed both in the time domain and the frequency domain. For vibration and ES data analysis, root mean square (RMS) is employed as a quick and cost-effective method, providing information of the overall trend of the signals. However, it may have limitations in detecting incipient defects and can be influenced by other sources of vibration such as unbalance and misalignment. In some situations, the peak amplitude and crest factor (peak-to-RMS ratio) can offer an earlier indication of defects.

These time-domain parameters were generated over a 500-cycles window per 200,000 cycles.

Before conducting frequency domain analysis, envelope analysis was used to extract the periodic impacts from the modulated random noise. This was achieved by applying a high pass filter to remove low-frequency components, followed by rectification and subsequent utilization of a low pass filter. The envelopes of the vibration and ES signals were left whose frequency corresponds to the repetition rate of defects. The frequency-domain analysis of the vibration and ES data was based on fast Fourier transformation (FFT) spectrum analysis. In the case of a developing fault on the specimens, increasing amplitudes at frequencies associated with the rotating characteristic frequencies would be observed.

AE data processing also involved both the time-domain and frequency domain analysis. Two time-domain parameters, AE counts and root mean square (RMS) were calculated and analysed. The AE counts represented the number of times the AE signal exceeded the threshold, which was set at 30% of the peak amplitude [15]. These time-domain parameters were generated over a 10-cycles window per 200,000 cycles. A representation of the frequency content of a signal was provided by the estimation of the power spectral density (PSD). The PSD estimate is derived by multiplying the amplitude of the FFT by its complex conjugate and normalising it with respect to the frequency bin width. In this study, the PSD estimate was computed using the Welch method [16]. The data acquisition and processing system for the three signals is illustrated in Figure 4.

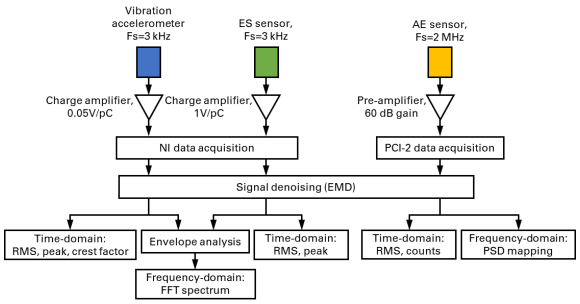

Figure 4. Schematic diagram of data acquisition and processing system

2.4. Test Conditions and Execution

Two tests conducted on the TE74 twin-disc tribometer are presented in this paper. The test conditions applied in the tests are shown in Table 1. Test 1 served as a baseline test and was anticipated to result in mild wear. Conversely, Test 2 was designed to induce more severe surface contact by increasing the roughness of Disc 2, thereby producing pitting fatigue. The test conditions were determined based on pervious studies [17, 18] where pitting fatigue was successfully produced.

Table 1. Test conditions for Test 1 and Test 2

No.	Disc 1 Rq (μm)	Disc 2 Rq (μm)	Entrainment speed (m/s)	Oil temp (°C)	Lambda	Slide-roll ratio (%)	Duration (million cycles)
1	0.03	0.04	0.612	100	1.15	-10	6
2	0.03	0.26	0.612	100	0.23	-10	6

Before and after the tests, the specimens were ultrasonically cleaned with 2-propanol for 10 minutes and dried with high pressure air. An Alicona G4 Infinite Focus profiler and a JSM-7200F scanning electron microscope (SEM) were used to inspect pitting topography and analyse pitting mechanisms.

3. Results and Discussion

3.1. Observation of Pitting Morphology

Post-test inspections were conducted using the Alicona profiler on the discs from Test 1 and Test 2 and the results are presented in Figure 5. Figure 5 (a) and (b) revealed that only mild wear along the rolling-sliding direction was produced on both discs from Test 1 without significant pitting or severe damage observed. In contrast, in Test 2, pitting with a width ranging from 150 to 800 μm was visible on Disc 1, as depicted in Figure 5 (c), while no apparent damage was found on Disc 2 as seen in Figure 5 (d).

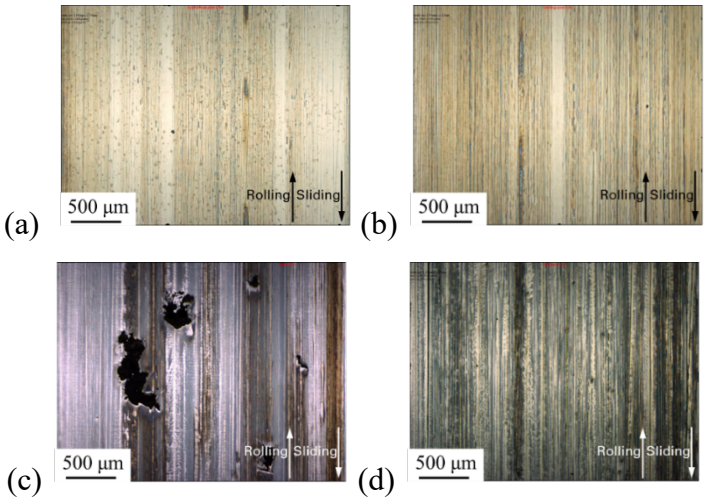

Figure 5. Surface topography images of (a) Disc 1 in Test 1 (b) Disc 2 in Test 1 (c) Disc 1 in Test 2 (d) Disc 2 in Test 2

These different failure modes can be attributed to different surface roughness combinations. The formation of pitting on Disc 1 in Test 2 was attributed to the rough surface of Disc 2. The findings agree with previous studies [17, 19], which have demonstrated that a smooth-rough contact configuration promotes the development of surface-initiated pitting on the smooth surfaces. The likely explanation for this is the stress history resulting from the fatigue micro-cycles is imposed by the dominant rougher surface upon the smoother one [17, 20].

To study the mechanism behind the formation of pitting, the surface and subsurface pitting morphology were examined using the JSM-7200F SEM. Figure 6 shows representative examples of pitting on surface and cross section views. As shown in Figure 6 (a), on the surface the pit was characterised by the separation of fine flakes or plates of the embrittled metal. The cross-section view shown in Figure 6 (b) was obtained by cutting through the centre of the wear tracks along the rolling/sliding direction. It is evident that the crack originated from the surface and generally propagated into the material. When the crack reached a critical length or depth, it branched toward the original surface, resulting in the removal of a section of surface material and generating pits with a saw-tooth bottom appearance, measuring approximately 20-30 μm in depth. This failure

mechanism is commonly observed in rolling element bearings where sliding occurs between the contacting surfaces [1, 21].

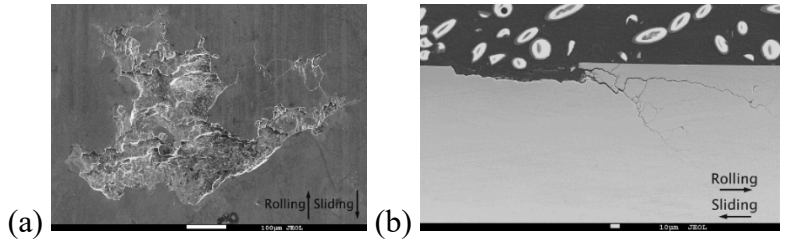

Figure 6. SEM observations of pitting on (a) surface and (b) cross section

To observe the progression of pitting, Test 2 was conducted two additonal times but halted at 1.5 million cycles and 3 million cycles respectively. The surface topography of Disc 1 at these three specific time points (1.5, 3, and 6 million cycles) is shown in Figure 7. Observations revealed that cracks with a length of 50 μm initiated around or just before 1.5 million cycles. By 3 million cycles, the number of cracks increased and they had developed into pits with widths of tens of microns. After 6 million cycles, there was a notable increase in the pitted area, indicating significant expansion and growth of the pits.

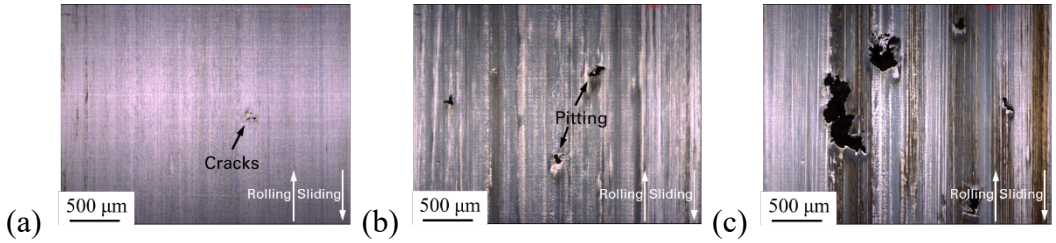

Figure 7. Surface topography images of Disc 1 at (a) 1.5 million cycles (b) 3 million cycles (c) 6 million cycles

3.2. Vibration Signal Analysis

Parameters such as RMS, peak amplitude, and crest factor were chosen for the time-domain analysis of the vibration signal. A comparison of these parameters between Test 1 and Test 2 was illustrated in Figure 8. It is evident that in Test 1, all three parameters exhibited lower values compared to Test 2, and no noticeable changes were observed during the test. In Test 2, the three parameters exhibited high values in the initial 0.6 million cycles, which may indicate the running-in stage. Running-in involves the interference of initial surface roughness, leading to the plastic deformation of surface asperities which generates dynamic stress fields and serves as vibration sources [22]. Following this stage, the RMS value slightly increased from 0.6 million cycles to 4 million cycles without displaying a significant change. This suggested that the machine was operating with slowly progressing faults. However, between 2.8 to 3.6 million cycles, the peak amplitude and crest factor demonstrated an upward trend, potentially indicating the initiation of faults. This may because the presence of a local fault produced short bursts of high energy which increased the peak level of the vibration signal but has little influence on the RMS level. As the faults continued to progress, more peaks were generated, eventually leading to a reduction in the crest factor but an increase in the RMS. In other words, the spikes indicated by the peak amplitude and crest factor may imply

incipient defects, whereas the high energy level given by the RMS may indicate the massive formation of severe defects.

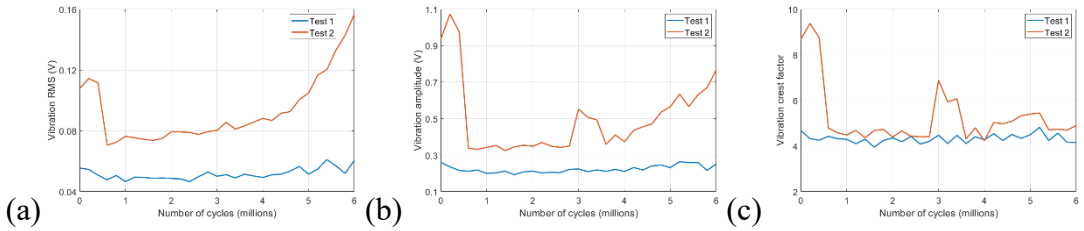

Figure 8. Vibration (a) RMS (b) peak amplitude (c) crest factor during Test 1 and Test 2

To locate the source of vibration, frequency-domain analysis was employed. Frequency-versus-time waterfall plots were generated using FFT as shown in Figure 9. Given that the rotating speed of Disc 1 was 600 rpm, corresponding to a frequency to 10 Hz, the pass frequency of defects on Disc 1 was also 10 Hz. In Test 1, despite the presence of minor peaks indicating the slow progression of mild wear, no significant changes were observed. In Test 2, discrete peaks at 10 Hz, aligned with the pass frequency of Disc 1, and its harmonics were visible at the beginning of the test which indicated the running-in stage. Subsequently, the peaks disappeared until 3 million cycles when they re-emerged and continued to grow until the end of the test. These peaks occurred at the pass frequency of Disc 1 and its harmonics, confirming the source of vibration was the occurrence of defects on Disc 1. Considering the disc surface inspections in Section 3.1, the defects were identified as pitting.

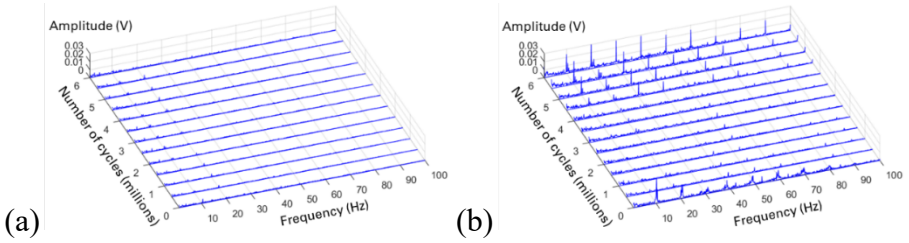

Figure 9. Frequency versus time waterfall plots of (a) Test 1 and (b) Test 2

It can be summarised that the vibration signal provided insights into the progression of pitting. The findings indicate that running-in occurred during the initial 0.6 million cycles, followed by the pitting initiation between 2.8 to 3.6 million cycles. Subsequently, there was a continuous development of extensive pitting until the end of the test.

3.3. AE Signal Analysis

Two typical AE time-domain features, RMS and counts were employed to identify and classify AE signals as shown in Figure 10. In Test 1, these two parameters displayed low values and slowly increased until the end, indicating the slow progression of mild wear. In Test 2, the running-in stage was characterised by the high level of these two parameters in the first 0.6 million cycles, which corresponded to the vibration analysis. Subsequently, the RMS and counts entered a constant steady state stage until 3.6 million cycles. However, it is worth noting that a rise in these parameters was observed at 1.8 million cycles, which be attributed to the release of energy and elastic waves resulting from

pitting initiation. After 3.6 million cycles. the parameters increased and remained high until the end of the test, indicating the presence of developed pitting.

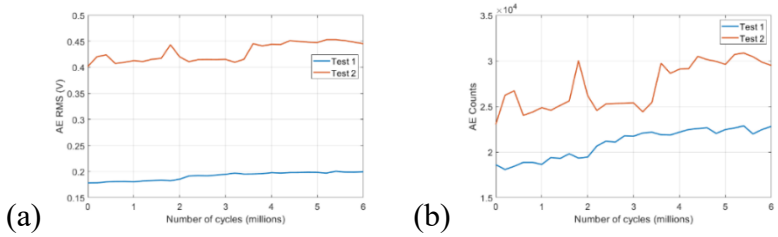

(a) (b)

Figure 10. AE (a) RMS (b) counts during Test 1 and Test 2

PSD maps of these two tests were displayed in Figure 11. In Test 1, a slight increase in energy was observed in the frequency range of 0.15 to 0.3 MHz after 2.4 million cycles which was due to the progression of mild wear. Conversely, Test 2 exhibited a more pronounced energy distribution across the frequency domain, suggesting more severe roughness contacts. Moreover, the increase in energy was identified between 0.15 to 0.3 MHz, and 0.45 to 1 MHz, during two distinct time intervals: from 1.6 to 2 million cycles and from 3.6 to 6 million cycles. These time points aligned with the periods when RMS and counts increased.

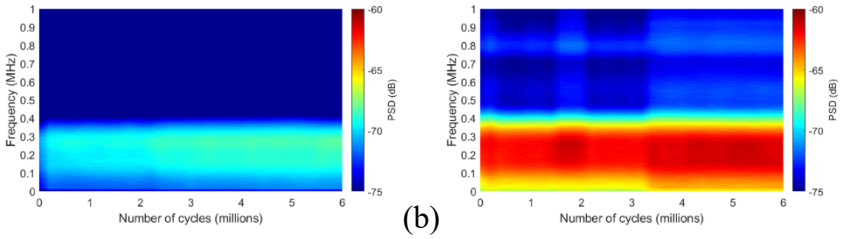

(a) (b)

Figure 11. AE PSD mapping of (a) Test 1 (b) Test 2

In reference [4], a correlation map was presented to demonstrate the relationship between the frequency spectrum of the AE signal and failure modes. In the current study, the observed increase in energy within the frequency range of 0.15 to 0.3 MHz aligned with the findings reported in [4], where fatigue damage on a bearing raceway was detected through the AE signal component within the 0.15 to 0.4 MHz. However, the difference in this study is that energy increased in a wider frequency range. This expanded frequency range could potentially be attributed to the presence of uniform distribution of pits, resulting in a broader impact on the frequency spectrum. To summarise, the analysis of the RMS, counts, and PSD maps of the AE signals allowed for the identification of the running-in stage, pitting initiation at 1.8 million cycles, and subsequent formation from 3.6 to 6 million cycles. Notably, AE was able to detect the presence of pitting at 1.8 million cycles, whereas vibration exhibited a delayed response at 2.8 million cycles. This highlights the advantage of AE in detecting pitting initiation at an earlier stage.

3.4. ES Signal Analysis

Figure 12 shows the RMS and peak amplitude values of the ES signals in Test 1 and Test 2. In Test 1, these two parameters displayed lower values compared to Test 2, and no noticeable changes were observed. In Test 2, consistent with the findings from the vibration and AE analysis, running-in was also captured by the ES sensor in the first 0.6

million cycles when both the RMS and peak amplitude were high. Subsequently, notable increases in the parameters were observed between 1.8 to 3.6 million cycles.

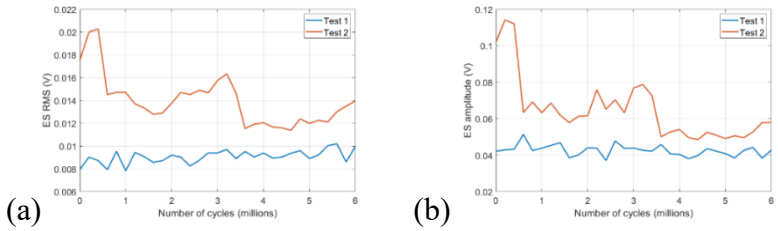

(a) (b)

Figure 12. ES (a) RMS (b) peak amplitude during Test 1 and Test 2

The FFT versus time waterfall plots shown in Figure 13 provide further insights. During Test 1, no significant changes were observed. In Test 2, peaks were identified at the pass frequency of Disc 1 and its harmonics between 2 to 4 million cycles, approximately corresponded to the period when the rise in RMS and peak amplitude was observed.

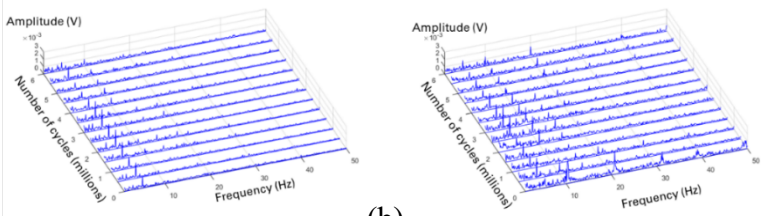

(a) (b)

Figure 13. FFT spectrums versus time of (a) Test 1 and (b) Test 2

The possible sources of electrostatic charge can be classified into four main areas: Tribo-charging, surface charge, tribo-emission, and debris formation [23, 24]. In this work, the charging mechanism primarily involved during the evolution of pitting was tribo-emission. Tribo-emission is defined as the emission of electrons, photons, ions and particles released during surface damage processing of solids, such as deformation, abrasion and fatigue cracking [23]. The increases in the time-domain parameters and peaks at the disc pass frequency in the frequency domain between 1.8 to 3.6 million cycles indicated that the pitting site was actively generating electrostatic charge during this period. This implies that the activity associated with pitting initiation was detected by the ES sensor as early as 1.8 million cycles. This detection occurred earlier than that achieved by the vibration accelerometer, highlighting the superior capability of the ES sensor in capturing pitting initiation activities at an earlier stage.

4. Conclusions

Experimental investigations have been conducted to detect and diagnose pitting fatigue on bearing steel discs. The acquired vibration, acoustic emission (AE), and electrostatic (ES) signals were analysed in both the time domain and frequency domain to effectively monitor the progression of pitting. The following conclusions were drawn based on the obtained experimental results.

1. The analysis of the vibration signals in the time domain provided valuable insights into the stages of running-in, pitting initiation, and pitting formation. The

frequency spectrum analysis identified the source of vibration was the pitting damage on Disc 1.

2. Similarly, the AE signal exhibited changes in both the time-domain parameters and the PSD map, reflecting the influence of running-in and the progression of pitting. The increase in RMS and counts, as well as the increase in energy across the certain frequency ranges, were observed during pitting initiation and formation. Notably, AE demonstrated an earlier detection of pitting initiation compared to vibration sensing.
3. Furthermore, the analysis of the ES signal demonstrated the sensitivity of the ES sensing technique to running-in and early pitting initiation. RMS and peak amplitude values captured pitting initiation, while the frequency spectrum displayed peaks at the disc pass frequency and its harmonics. The ES sensing technique also exhibited an earlier detection of pitting initiation when compared to vibration sensing.
4. Overall, these three sensing techniques proved to be sensitive to different aspects during the evolution of pitting fatigue. Pitting formation was more pronounced in the vibration signal analysis, while AE and ES tended to achieve an earlier detection of pitting initiation. Combining these technologies may offer a more comprehensive understanding of the pitting progression and mechanism.

Acknowledgements

The authors would like to thank Schaeffler Technologies AG & Co. KG, Herzogenaurach, Germany for providing financial support and test samples for this work.

References

1. Corni, I., et al., *Characterization and mapping of rolling contact fatigue in rail-axle bearings.* Engineering Failure Analysis, 2017. **82**: p. 617-630.
2. Amarnath, M. and I. Praveen Krishna, *Experimental investigations to assess surface contact fatigue faults in the rolling contact bearings by enhancement of sound and vibration signals.* Journal of Nondestructive Evaluation, 2019. **38**: p. 1-23.
3. Feng, K., et al., *A novel vibration indicator to monitor gear natural fatigue pitting propagation.* Structural Health Monitoring, 2023: p. 14759217221142622.
4. Hase, A., *Early detection and identification of fatigue damage in thrust ball bearings by an acoustic emission technique.* Lubricants, 2020. **8**(3): p. 37.
5. Rahman, Z., et al., *Incipient damage detection and its propagation monitoring of rolling contact fatigue by acoustic emission.* Tribology International, 2009. **42**(6): p. 807-815.
6. Hutt, S., A. Clarke, and H. Evans, *Generation of Acoustic Emission from the running-in and subsequent micropitting of a mixed-elastohydrodynamic contact.* Tribology International, 2018. **119**: p. 270-280.
7. Wirtz, S.F., et al. *Frequency-based damage detection of spur gear using wavelet analysis*. in *8th European Workshop on Structural Health Monitoring (EWSHM 2016)*. 2016.
8. Yan, Y., et al., *Electrostatic sensors–Their principles and applications.* Measurement, 2021. **169**: p. 108506.

9. Zhang, Y., H. Zuo, and F. Bai, *Feature extraction for rolling bearing fault diagnosis by electrostatic monitoring sensors.* Proceedings of the Institution of Mechanical Engineers, Part C: Journal of Mechanical Engineering Science, 2015. **229**(10): p. 1887-1903.
10. Harvey, T., R. Wood, and H. Powrie, *Electrostatic wear monitoring of rolling element bearings.* Wear, 2007. **263**(7-12): p. 1492-1501.
11. Powrie, H., et al. *Electrostatic charge generation associated with machinery component deterioration*. in *Proceedings, IEEE Aerospace Conference*. 2002. IEEE.
12. Huang, N.E., et al., *The empirical mode decomposition and the Hilbert spectrum for nonlinear and non-stationary time series analysis.* Proceedings of the Royal Society of London. Series A: mathematical, physical and engineering sciences, 1998. **454**(1971): p. 903-995.
13. Sadoughi, M. and C. Hu, *Physics-based convolutional neural network for fault diagnosis of rolling element bearings.* IEEE Sensors Journal, 2019. **19**(11): p. 4181-4192.
14. Geropp, B., *Envelope analysis-a signal analysis technique for early detection and isolation of machine faults.* IFAC Proceedings Volumes, 1997. **30**(18): p. 977-981.
15. Morhain, A. and D. Mba, *Bearing defect diagnosis and acoustic emission.* Proceedings of the Institution of Mechanical Engineers, Part J: Journal of Engineering Tribology, 2003. **217**(4): p. 257-272.
16. Welch, P., *The use of fast Fourier transform for the estimation of power spectra: a method based on time averaging over short, modified periodograms.* IEEE Transactions on audio and electroacoustics, 1967. **15**(2): p. 70-73.
17. Vrček, A., et al., *Micro-pitting damage of bearing steel surfaces under mixed lubrication conditions: effects of roughness, hardness and ZDDP additive.* Tribology International, 2019. **138**: p. 239-249.
18. Lainé, E., A. Olver, and T. Beveridge, *Effect of lubricants on micropitting and wear.* Tribology International, 2008. **41**(11): p. 1049-1055.
19. Morales-Espejel, G.E. and V. Brizmer, *Micropitting modelling in rolling–sliding contacts: application to rolling bearings.* Tribology Transactions, 2011. **54**(4): p. 625-643.
20. Kim, T. and A. Olver, *Stress history in rolling–sliding contact of rough surfaces.* Tribology International, 1998. **31**(12): p. 727-736.
21. Sadeghi, F., et al., *A review of rolling contact fatigue.* Journal of Tribology, 2009. **131**.
22. Halme, J. and P. Andersson, *Rolling contact fatigue and wear fundamentals for rolling bearing diagnostics-state of the art.* Proceedings of the Institution of Mechanical Engineers, Part J: Journal of Engineering Tribology, 2010. **224**(4): p. 377-393.
23. Powrie, H., L. Wang, and R. Wood, *Electrostatic monitoring of tribo-contacts: then and now.* WCCM 2017, 2017.
24. Morris, S., et al., *Use of electrostatic charge monitoring for early detection of adhesive wear in oil lubricated contacts.* J. Trib., 2002. **124**(2): p. 288-296.